Check for updates

RESEARCH ARTICLE

LASER & PHOTONICS REVIEWS

www.lpr-journal.org

# Integrated Photonics and Electronics for High-Speed Quantum Key Distribution

*Zhao-Yuan Chen, Xin-Zhe Wang, Yang Li,* Yu-Ang Wang, Chao-Ze Wang, Li-Kang Zhang, Yan-Fei Liu, Wen-Qi Cai, Juan Yin, Ji-Gang Ren, Feihu Xu, Sheng-Kai Liao,* and Cheng-Zhi Peng*

**Quantum key distribution (QKD) has made significant advancements over the past few decades and is gradually transitioning from laboratory to industrial domain. This transformation process poses urgent demands for integrated, cost-effective, and mass-producible QKD devices. Here, by interfacing a laser diode, a QKD encoding photonics chip, and their associated electronics driver chips, the QKD transmitter has been condensed from several bulky discrete components to integrated modules with dimensions of a few centimeters, while the modulation rate of the transmitter has been enhanced to 3.33 GHz. Based on this transmitter, QKD is demonstrated over a 100 km standard fiber channel, capable of generating secure keys at a record high key rate of 2.82 Mbps over this distance. This work demonstrates the feasibility of high-speed integrated QKD transmitters, thereby further propelling the research on QKD in practical applications.**

## 1. Introduction

The advancement of quantum computing is posing substantial challenges to information security and privacy. In response to this, quantum key distribution (QKD) is emerging as a physically secure alternative to classical cryptography methods, capitalizing on the principles of quantum mechanics.[1,2] Recent years have witnessed remarkable progress in QKD, with the range of secure key distribution extending from mere centimeters to thousands of kilometers.[3–12] Furthermore, experiments have transitioned from controlled laboratory environments to practical, real-world applications.[13–21] It is evident that the realm of QKD is undergoing a significant transformation, moving from the confines of the laboratory into the realm of practical application, with the emergence of the quantum communication industry.

The industrial development of quantum communication has spurred research in integrated QKD devices. Photonics integrated circuits (PIC) technology, with its high integration, scalability for mass production, cost-effectiveness, and high stability, represents a crucial pathway for the practical implementation of QKD. In 2016, Ma et al. published their research on silicon photonics QKD transmitter chip.[22] They designed a polarization-encoded chip architecture compatible with the complementary metal oxide semiconductor (CMOS) platform, integrating the intensity modulator (IM) and polarization modulator (PM) required for QKD transmitter on one chip. This breakthrough led to a surge in PIC-based QKD research. In just a few years, researchers leveraged PIC technology to create integrated QKD chips with different protocols: BB84,[23–26] measurement-device-independent,[27,28] and continuous-variable[29] QKD; and different encoding schemes: polarization,[30,31] time-bin,[23–25,27] and high-dimensional[32] encoding. Decoding chips corresponding to different encoding methods have also emerged successively.[33–39] They successfully conducted experimental verification over both optical fiber[40] and free-space channels.[41] Recently, Li has achieved record-breaking secure key rate (SKR) using high-performance single-photon detectors in conjunction with the high bandwidth features of PIC.[42]

Researchers have made significant progress in the development of QKD PICs. However, researches in the integrated driving of these PICs have lagged behind in comparison. The majority of these research efforts have employed arbitrary waveform generator or printed circuit board technologies to drive

Z.-Y. Chen, X.-Z. Wang, Y. Li, Y.-A. Wang, C.-Z. Wang, L.-K. Zhang, W.-Q. Cai, J. Yin, J.-G. Ren, F. Xu, S.-K. Liao, C.-Z. Peng
Hefei National Research Center for Physical Sciences at the Microscale and School of Physical Sciences
University of Science and Technology of China
Hefei 230026, China
E-mail: liyang9@ustc.edu.cn; skliao@ustc.edu.cn

Z.-Y. Chen, X.-Z. Wang, Y. Li, Y.-A. Wang, C.-Z. Wang, L.-K. Zhang, W.-Q. Cai, J. Yin, J.-G. Ren, F. Xu, S.-K. Liao, C.-Z. Peng
Shanghai Research Center for Quantum Science and CAS Center for Excellence in Quantum Information and Quantum Physics
University of Science and Technology of China
Shanghai 201315, China

Z.-Y. Chen, X.-Z. Wang, Y. Li, Y.-A. Wang, C.-Z. Wang, L.-K. Zhang, W.-Q. Cai, J. Yin, J.-G. Ren, F. Xu, S.-K. Liao, C.-Z. Peng
Hefei National Laboratory
University of Science and Technology of China
Hefei 230088, China

Z.-Y. Chen, Y.-F. Liu
Xi'an Research Institute of High Technology
Xi'an 710025, China

The ORCID identification number(s) for the author(s) of this article can be found under https://doi.org/10.1002/lpor.202501080

**DOI: 10.1002/lpor.202501080**

 © 2025 Wiley-VCH GmbH

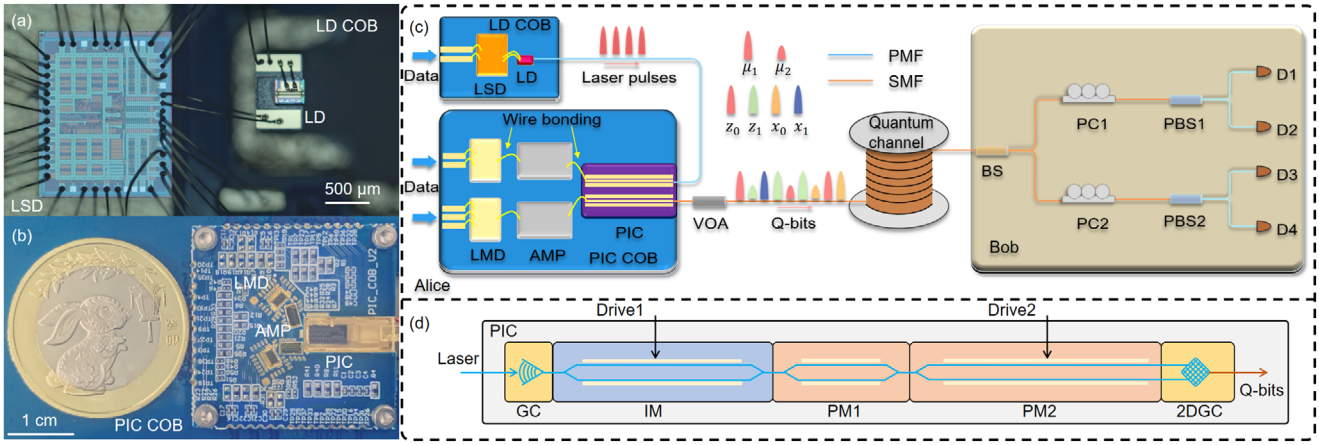



**Figure 1.** a) Photo of the LD COB module. The laser driver chip (LSD, left) and the laser diode chip (LD, right) are directly connected by wire bonding. The size of the entire module is 1.5 × 1.5 cm. b) Photo of the PIC COB module. The PIC COB module integrates a QKD PIC, two modulator driver chips (LMD), and two amplifiers (AMP). The interconnection between the chips is also implemented using direct wire bonding. The size of the entire module is 3 × 3 cm. The interconnection between COB and PCB was achieved through metallized castellated holes patterned along the module edge. c) QKD Experimental setup. VOA, variable optical attenuator; PMF, polarization-maintaining fiber; SMF, single-mode fiber; BS, beam splitter; PC, polarization controller; PBS, Polarization beam splitter; D, detector. d) Schematic of the QKD PIC. GC, grating coupler; IM, intensity modulator; PM, polarization modulator; 2DGC, 2D grating coupler.

the PIC. The bulky driving equipment have posed a significant obstacle to fully utilizing the advantages of integration in PIC. In 2022, Zhu et al. proposed a QKD scheme utilizing integrated electronics chips to drive PICs, further advancing the practical application of integrated QKD systems.[43] Their scheme utilized separate chips and devices, with a modulation rate of 312.5 MHz, achieving a SKR of 42.7 kbps on a 100 km fiber channel. Recently, Sax et al. introduced a high-speed QKD system that combines both integrated photonics and electronic chips. Their transmitter, consisting of an integrated QKD coding module and independent laser and filter, worked at 2.5 GHz clock rate and achieved a SKR of 9.4 kbps over a 200 km fiber channel.[44]

Here, to address the challenge of interfacing the integrated quantum photonics chip with its electronic driver chip, we introduce an integrated QKD transmitter utilizing chip-on-board (COB) hybrid packaging technology. This technology allows us to co-package the QKD PIC and laser diode (LD) chip together with their electronics driving chips through wire bonding, rather than connecting discrete chips and devices with cables.[43,44] This not only reduces the QKD transmitter volume, but also improves bandwidth limitations associated with interconnects between photonics and electronics chips. We constructed a QKD transmitter using a LD COB module and a PIC COB module, achieving a modulation rate of 3.33 GHz using the decoy-state BB84 protocol with polarization encoding, which is the fastest integrated QKD system to our knowledge. We conducted QKD experiments under different channel losses, obtaining a record high SKR of 2.82 Mbps over a 100 km optical fiber channel. Our work provides a feasible approach for further enhancing the integration level and modulation rate of QKD systems, thus advancing the research process towards the industrialization of integrated QKD system.

## 2. Experimental Setup

The QKD transmitter consists of two modules: the LD COB module and the PIC COB module. **Figure 1**a,b show photographs of two COB modules. The LD COB module co-packages a 1550.12 nm distributed feedback LD and a laser driver chip (LSD),[45] and the PIC COB module co-packages a QKD PIC,[43] two modulator driver chips (LMD),[46] and two amplifiers to realize quantum states preparation. The LSD and LMD chips were designed and manufactured using 180 nm SiGe bipolarCMOS technology, which incorporates high-performance npn heterojunction bipolar transistors capable of achieving transit frequencies of up to 240 GHz (detailed design specifications can be found in ref. [46]). These chips have a compact size of 1.35 × 2.25 $mm^2$. The PIC was fabricated by a commercial silicon photonics foundry using a 180 nm silicon-on-insulator process and features a footprint of 2.95 × 5.80 $mm^2$, with a modulator half-wave voltage of 3.5 V. The LD is a commercially used chip made of InP material. The signal interconnection between chips is achieved through standard gold wire bonding processes (as shown in microscope photo Figure 1a), which allows us to integrate all the key photonics and electronics components of the QKD transmitter into a COB packaging module. By incorporating spacers between chips of different thicknesses to achieve coplanarity at both bonding ends, we ensure uniform stress distribution across the bond wires, further enhancing their mechanical reliability. This wire bonding approach offers significant electrical advantages by eliminating the parasitic parameters associated with PCB traces between chips, thereby optimizing impedance matching in the signal transmission path and improving high-frequency driving signal integrity. Through compact layout design, we minimize the bonding wire length to reduce impedance mismatch and cross-talk effects caused by the lack of reference planes. This significantly reduces the


© 2025 Wiley-VCH GmbH

18638899, 0, Downloaded from https://onlinelibrary.wiley.com/doi/10.1002/lpor.202501080 by Shenglai Liao - University Of British Columbia , Wiley Online Library on [29/09/2025]. See the Terms and Conditions (https://onlinelibrary.wiley.com/terms-and-conditions) on Wiley Online Library for rules of use; OA articles are governed by the applicable Creative Commons License

size of the QKD transmitter, with the entire PIC COB module being only the size of a coin as shown in Figure 1b. This small module co-packages the integrated photonics chip and electronics driver chips required for QKD, requiring only an external power source and data input to operate. Moreover, direct wire bonding eliminates the need for additional interconnection devices between chips, reducing the impact of parasitic parameters on the quality of the driving signals. This allows our transmitter to operate at a high modulation speed of 3.33 GHz.

Figure 1c illustrates a schematic diagram of the entire QKD experimental setup. The LSD receives a current mode logic (CML) data signal and drives the LD in gain-switch mode to produce weak coherent pulses with random phase in 3.33 GHz clock rate. Two LMD chips convert the input multi-channel CML data into multi-amplitude driving signals to control the IM and PM on the PIC. Figure 1d is a schematic of the QKD PIC. The laser pulses are input into the PIC through a grating coupler and are then modulated into different intensity states using a Mach-Zehnder interferometer (MZI) IM. The decoy states theory is an essential component in the practical application scenarios of current QKD systems with weak coherent pulses.[47,48] We applied a 1-decoy state protocol, and the average photon numbers of two intensities are $\mu_1$ and $\mu_2$ with probabilities of $P_{\mu_1}$ and $P_{\mu_2}$ respectively. Subsequently, a two-stage PM implements path and phase encoding. The 2D grating coupler (2DGC) transforms the phase into polarization states and outputs them from the chip. Since the BB84 protocol only requires four quantum states, here we apply a DC bias to PM1 and a high-speed modulation signal to PM2 to encode photons in Z and X basis with probabilities of $P_Z^A$ and $P_X^A$, respectively. The prepared quantum bits (Q-bits) are attenuated through a variable optical attenuator (VOA) and then transmitted through the quantum channel to the receiver end.

The receiver Bob possesses a BB84 polarization decoding setup. It includes a beam splitter with splitting ratio of $P_Z^B/P_X^B$ for passive basis selection, two polarization controllers for compensating polarization states in the optical fiber, two polarization beam splitters for polarization state decoding, and four superconducting nanowire single-photon detectors (SNSPD) for photon detection. The detector efficiency of the SNSPD is set to approximately 75%–80%. Under this condition, the time jitter of the detector is less than 65 ps, with a dark count rate of about 25 Hz for each channel.

## 3. Results

We initially tested the laser pulse waveform using a 12 GHz bandwidth photoreceiver (Newport, model 1544-B) and a 36 GHz bandwidth oscilloscope (Teledyne LeCroy LabMaster 10 Zi 36 GHz Systems) to validate the performance of the LD COB module. We gathered over 1000 sets of waveform data, illustrated in **Figure** 2a. The average full-width at half maximum (FWHM) of the laser pulses is merely 50 ps, attaining a level comparable to discrete component laser equipment. This capability is adequate to support a high-speed QKD experimental setup operating at 3.33 GHz.

In this system, we implemented the decoy-state efficient BB84 protocol, involving the preparation of two intensity states

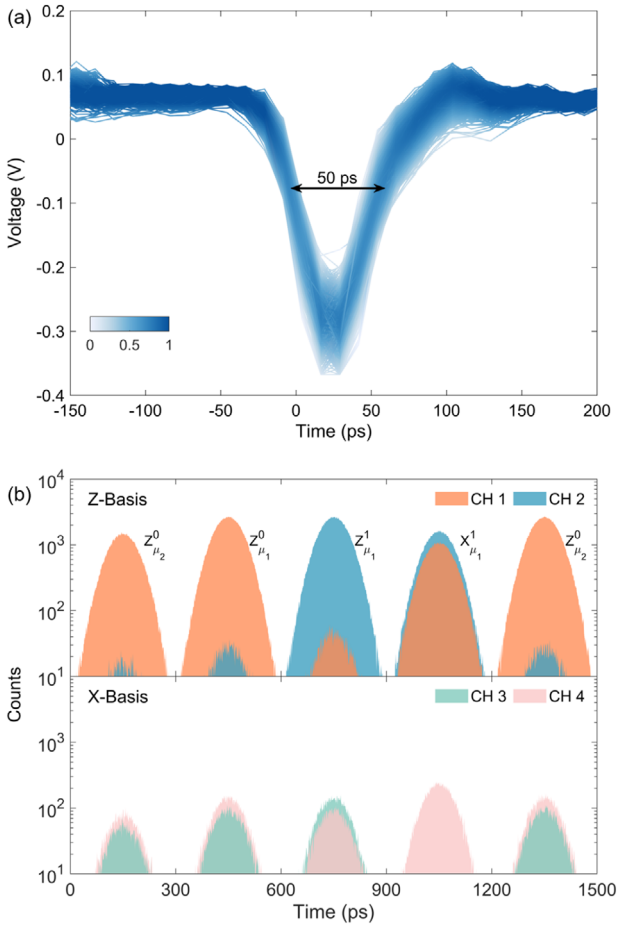



**Figure 2.** a) The collected laser pulse waveform at a clock rate of 3.33 GHz. The photoreceiver is negative gain responsive, resulting in a negative pulse signal voltage. b) Excerpt of the recorded histogram of four detectors. The upper plot displays histograms for channel 1 (orange) and channel 2 (blue) of the Z-basis detectors. The lower plot displays histograms for channel 3 (green) and channel 4 (pink) of the X-basis detectors. The pulses labeled Z and X represent the basis for quantum state preparation. The superscripts 0 and 1 represent bit values, while the subscripts $\mu_1$ and $\mu_2$ indicate intensity states.

and four polarization states. The average numbers of photons for the two intensity states are specified as $\mu_1 = 0.38$ and $\mu_2 = 0.21$, with corresponding probabilities $P_{\mu_1} = 0.7$ and $P_{\mu_2} = 0.3$. Alice and Bob adopt the Z-basis to prepare and measure Q-bits, with a probability of $P_Z^A = P_Z^B = 0.92$. Figure 2b illustrates the statistical distribution histogram of photon counts, with the upper and lower plots representing counts from detectors aligned with the Z-basis and X-basis, respectively. Based on the statistical results shown in Figure 2b, the average photon numbers for the two intensity pulses are calculated to be 0.383 and 0.212, with bit error rates of 1.34% and 1.76% under the Z-basis and X-basis, respectively. This precision enables us to accurately prepare intensity and polarization states.

We conducted QKD experiments under varying lengths of optical fiber and channel attenuation. We utilized the finite-key the-


© 2025 Wiley-VCH GmbH

18638899, 0, Downloaded from https://onlinelibrary.wiley.com/doi/10.1002/lpor.202501080 by Shenglai Liao - University Of British Columbia , Wiley Online Library on [29/09/2025]. See the Terms and Conditions (https://onlinelibrary.wiley.com/terms-and-conditions) on Wiley Online Library for rules of use; OA articles are governed by the applicable Creative Commons License

ory for 1-decoy state to generate secure keys.[49] The secure key (SK) extraction formula is as follows:

$$SK = s^{l}_{Z,0} + s^{l}_{Z,1}(1 - h(\phi^{u}_{Z})) - f \times n_{Z} \times h(E_{Z}) - 6log_{2}(19/\epsilon_{sec}) - log_{2}(2/\epsilon_{cor}) \quad (1)$$

where $s^{l}_{Z,1}$ ($s^{l}_{Z,0}$) is the lower bound on the number of single-photon contributions (vacuum state contributions); $\phi^{u}_{Z}$ is the upper bound on the single-photon phase error rate; $h$ is the binary entropy function; $f = 1.12$ is the efficiency of the error correction code; $n_{Z}$ is the sifted key length in the Z-basis; $E_{Z}$ is the quantum bit error rate (QBER) in the Z-basis; $\epsilon_{sec} = 10^{-10}$ and $\epsilon_{cor} = 10^{-15}$ are the secrecy and correctness parameters.

In **Figure 3a**, the blue solid line represents the relationship between the SKR and channel attenuation obtained through simulation based on the experimental configuration. The solid and hollow stars in the figure represent the experimental results under simulated channels with standard optical fibers and equivalent attenuation, respectively. We obtained a SKR of 2.82 Mbps and a QBER of 1.43% within 135 s acquisition time (block size $n_{Z} = 10^{9}$) on a 100 km standard optical fiber channel (19.07 dB). This is the highest SKR ever recorded at this distance. In other experiments, in order to balance SKR and acquisition time, we fixed the block size at $10^{8}$. The SKRs obtained at distances of 130 km (24.5 dB), and 150 km (28.6 dB) are 753 kbps and 289 kbps, with QBER (plotted in the sub-figure of Figure 3(a)) of 1.47% and 1.45%, respectively. To validate the key distribution performance at longer distances, we simulated the quantum channel using equivalent attenuation. At attenuations of 35, 40, 45, and 50 dB, we achieved SKRs of 72.7, 21.3, 6.0, and 1.4 kbps, with QBERs of 1.36%, 1.39%, 1.48%, and 1.70% respectively. Comparison between recent PIC QKD works based on BB84 protocol and our results is plotted in Figure 3a. Our system achieved the highest SKR on same channel attenuation, leveraging the advantage of high-speed modulation. Moreover, secure keys can still be obtained even with channel attenuation exceeding 50 dB.

To validate long-term stability of the system, we conducted a continuous 200-min QKD experiment under a channel loss of 25 dB. We configured the system parameters and the decoding end before the experiment. No further interventions were made during the experimental process. We divided the entire experimental process into 200 rounds, and in each round, the key extraction was performed using photons accumulated over a 45-s period as a block. The experimental results are plotted in Figure 3b. The average QBER for the entire experiment was 1.35%, with a standard deviation of 0.05%. The average secure data rate was 710 kbps, with a standard deviation of 17 kbps. Throughout the 200-min operation, the system remained in a consistently stable working state.

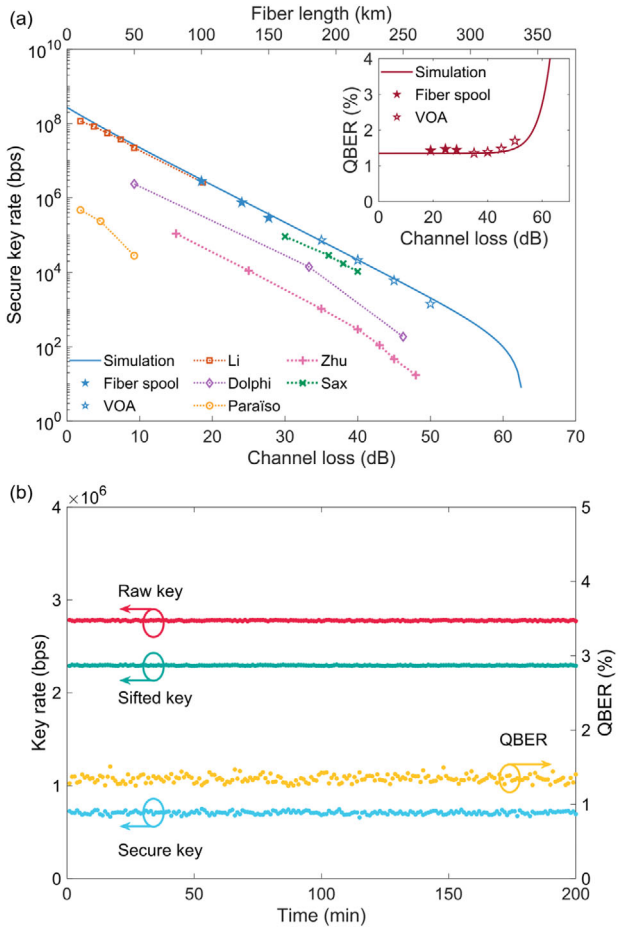



**Figure 3.** a) SKR and QBER results under different channel losses and fiber lengths. The blue solid line represents the relationship between the SKR and channel attenuation obtained through simulation based on our experimental configuration, while the red solid line is the simulated QBER under different channel losses. Solid stars represent data under optical fiber channels, while hollow stars represent the equivalent attenuation results. The square, diamond, and circle symbols represent SKR data under different lengths of optical fiber channels, sourced from references.[42,51,58] The plus and cross symbols represent SKR data under different channel attenuation, sourced from the references.[43,44] b) The results of long-term stability experiments. The red, green and cyan data points are the raw key, sifted key and SKR, and the yellow data points are QBER. Each data point represents the cumulative result of 45 s.

## 4. Conclusion and Discussion

In summary, we propose an advanced integration solution for the current QKD transmitter from the perspective of optoelectronics hybrid packaging technology. We integrate an LD chip, a quantum bit encoding chip, and the required electronics driver chips through COB packaging on a coin-sized PCB. The entire COB module incorporates all the hardware modules of the QKD transmitter, requiring only external power and data input to complete the QKD functionality. Our solution not only further reduces the size of the QKD transmitter but also eliminates the parasitic parameters introduced by intermediary devices through directly interconnecting the photonics and electronics chips. This enhances the modulation bandwidth, allowing us to achieve a modulation rate of 3.33 GHz.

To illustrate the progress of our work in the research of integrated QKD systems, we have compiled representative studies of integrated QKD systems from the past few years in **Table 1**. We have compared these studies in terms of modulation rate, coding scheme, integrated modules, QBER, and SKR. One of our contributions is increasing the modulation rate of the integrated


© 2025 Wiley-VCH GmbH

18638899, 0, Downloaded from https://onlinelibrary.wiley.com/doi/10.1002/lpor.202501080 by Shenglai Liao - University Of British Columbia , Wiley Online Library on [29/09/2025]. See the Terms and Conditions (https://onlinelibrary.wiley.com/terms-and-conditions) on Wiley Online Library for rules of use; OA articles are governed by the applicable Creative Commons License

**Table 1.** A List of High-Speed Integrated QKD Systems in Recent Years.

| Reference | Modulation rate (Hz) | Coding scheme | Laser | Encoder | Driver | Decoder | QBER (%) | SKR |
|---|---|---|---|---|---|---|---|---|
| T. K. Paraïso[25] | 1 G | Time-bin | ✓* | ✓ | — | — | 2.5 | 270 kbps @ 100 km |
| T. K. Paraïso[51] | 1 G | Time-bin | ✓ | ✓ | — | ✓ | 4.5 | 470 kbps @ 10 km |
| G. Zhang[59] | 2 G | Polarization | — | ✓ | — | ✓ | 0.9/1.34 | 868 kbps @ 20 km |
| C. X. Zhu[43] | 312.5 M | Polarization | — | ✓ | ✓ | — | 0.59 | 42.7 kbps @ 100 km |
| W. Li[42] | 2.5 G | Polarization | — | ✓ | — | — | 0.56 | 2.6 Mbps @ 101 km |
| R. Sax[44] | 2.5 G | Time-bin | — | ✓ | ✓ | ✓ | 0.9 | 9.4 kbps @ 202 km |
| J. A. Dolphin[58] | 1 G | Time-bin | ✓ | ✓ | — | ✓ | 0.66 | 2.37 Mbps @ 50 km |
| Lin[60] | 2.5 G | Time-bin | — | ✓ | — | ✓ | 0.53 | 10 Mbps @ 25 km |
| This work | 3.33 G | Polarization | ✓ | ✓ | ✓ | — | 1.43 | 2.82 Mbps @ 100 km |

*The check mark indicates that the integrated device is included in the system.

QKD transmitter to 3.33 GHz. Our waveform generator (Keysight 81134A), providing data signal input for the COB module, has a minimum signal period of 300 ps, directly determining our modulation rate of 3.33 GHz. At this modulation rate, the QBER is mainly limited by signal-to-noise ratio of the driving signal[46] and detection system jitter. The same phenomenon is observed in discrete QKD system with higher modulation rates. Grünenfelder achieved a modulation rate of 5 GHz with a QBER of 1.93%.[50] The SKR of this 5 GHz system over a 101 km fiber channel is only 392.7 kbps. While a faster system modulation rate is beneficial for increasing SKR, the accompanying rise in QBER tends to decrease it. Therefore, in our experimental setup, the scheme to improve SKR by further increasing the modulation rate has little effect (for details, see the Appendix). The crucial challenge lies in reducing the noise of the driving signal at high speed to enhance SKR by lowering QBER. To further increase the system modulation rate, the following measures can be implemented: optimizing the output signals of the EIC, employing ultra-narrow laser pulse technology, and reducing detector jitter.

Another contribution is to further integrate the QKD transmitter (Table 1). We believe a complete QKD transmitter should be capable of converting digital signals into quantum states and transmitting them. Therefore, lasers, quantum encoders, and their corresponding driver circuits are essential components. Currently, the research at the chip level is the most mature, with an abundance of references on chips related to various protocols and encoding schemes. Conversely, there is relatively limited research at the integrated module level, and even fewer studies exist at the integrated system level. For instance, ref. [42] achieved a remarkably high SKR (115.8 Mbps @ 10 km fiber) using PIC with a 2.5 GHz modulation rate. While utilizing a PIC for QKD encoding transmission, their system retained discrete electronic drivers. In this work, we have achieved the full integration of all these necessary components for the QKD transmitter by directly interconnecting them, and further promote the development of integration from the level of QKD module. Chip-based integrated systems offer distinct advantages beyond high integration density. Crucially, they also enable mass production capabilities. The stable, reliable fabrication processes and relatively lower costs represent an essential pathway for QKD's transition to industrial-scale commercialization.

From a system perspective, a complete QKD system should include not only the transmitter but also a digital signal processor, a quantum random number generator, a receiver, and detectors. The quantum communication system demonstrated by Paraïso integrates all the mentioned modules, representing a mature and operational integrated solution for quantum communication.[51] Our emphasis of future research would be placed on the development of other integrated QKD modules and systems. For instance, there remains an absence of a fully integrated QKD decoder in our system. Despite significant advances in integrated decoding chips, they still suffer from relatively high optical losses. Exploring novel low-loss materials, such as thin-film lithium niobate (TFLN), SiN and borosilicate glass,[35,38,52] may provide a critical pathway to overcome this bottleneck. Additionally, integrated single-photon detection systems require further development. While the core components of SNSPD have achieved on-chip integration,[53] their cryogenic operating temperatures remain dependent on external cooling systems. In contrast, detectors based on semiconductor materials have made notable progress in integration.[54,55] Recent research has achieved room-temperature operation using a waveguide-coupled silicon single-photon avalanche diodes, opening new possibilities for practical applications.[56,57] Techniques such as monolithic integration and optoelectronic hybrid packaging can be employed to modularize various functionalities of QKD. Subsequently, leveraging solutions like system in package and embedded systems will further advance the integration of QKD systems. With further improvements in the integration of QKD terminals, they can be deployed not only in fiber networks, but also on unmanned aerial vehicles or even satellite platforms for more practical and valuable application scenarios. From the perspective of quantum networks, higher integration is advantageous for the mass production of QKD nodes, aligning more closely with the requirements of industrial development.

## Appendix

In this section, we will discuss the effects of further increasing the modulation rate in our experimental system. In the discussion section, we stated that further increasing the modulation rate would lead to a rise in QBER, thereby resulting in limited contribution to the SKR. Actually, we categorize the sources of QBER into two components: i) degraded driving signal


© 2025 Wiley-VCH GmbH

18638899, 0, Downloaded from https://onlinelibrary.wiley.com/doi/10.1002/lpor.202501080 by Shenglai Liao - University Of British Columbia , Wiley Online Library on [29/09/2025]. See the Terms and Conditions (https://onlinelibrary.wiley.com/terms-and-conditions) on Wiley Online Library for rules of use; OA articles are governed by the applicable Creative Commons License

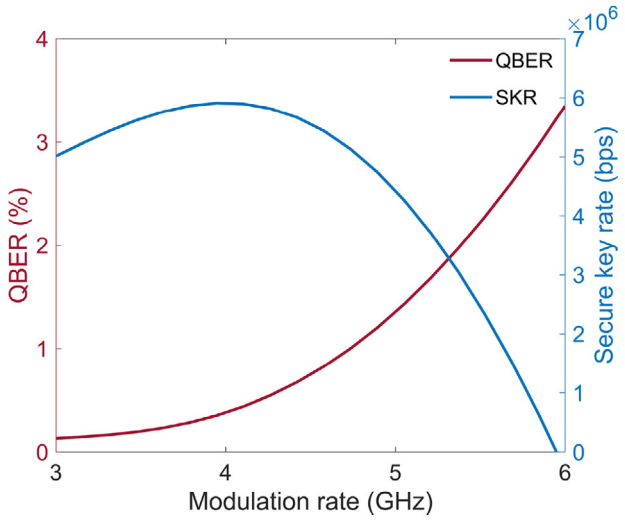



**Figure 4.** Simulation results of QBER and SKR under different modulation rates. The red curve represents the QBER with its vertical axis on the left, while the blue curve shows the SKR with its vertical axis on the right. At each modulation rate point, the counting gate width is set equal to the clock period.

noise ratio, and ii) timing-jitter-induced pulse overlap in detection. Here, we conducted a simulation to assess these effects.

We first simulated the output signal noise of the EIC driver chip at different modulation rates. Then, based on the method given in ref. [46], the encoding bit error rates caused by the driving signal at different modulation rates were calculated. On this basis, the influence brought by inter-symbol interference was evaluated to obtain the simulation results shown in **Figure 4**.

From the simulation results, it can be observed that within the 3 GHz to 4 GHz frequency range, the QBER rises relatively slowly. This is primarily because the pulse period still exceeds the laser pulse width (specifically the 1/100 intensity width of 240 ps), resulting in minimal inter-symbol interference from adjacent pulse overlap. The increase in QBER is mainly caused by the noise from EIC. Consequently, increasing the modulation rate within this range enhances the SKR. However, when the modualtion rate exceeds 4 GHz, the QBER rises sharply under the influence of these two factors. At this point, the negative impact of elevated QBER outweighs the positive effect of higher modulation rate, leading to a degradation in SKR. It is worth noting that the calculation results here used an ideal EIC simulated signal as the input for the computational model, so the obtained QBER is relatively small compared to experimental data, but the overall trend can serve as a reference.

## Acknowledgements

Z.-Y.C. and X.-Z.W. contributed equally to this work. The authors gratefully acknowledged Fu-Tian Liang for providing chip resources, the SJTU Pinghu Institute of Intelligent Optoelectronics for technical support, and the Information Science Laboratory Center of USTC for hardware/software services. This work was supported by the National Key Research and Development Program of China (Grant Nos. 2020YFA0309701, 2020YFA0309703, and 2022YFF0610100); the Shanghai Municipal Science and Technology Major Project (Grant No. 2019SHZDZX01); the Innovation Program for Quantum Science and Technology (Grant Nos. 2021ZD0300104 and 2021ZD0300108); the National Natural Science Foundation of China (Grant No. 12374475); and the Natural Science Basis Research Plan in Shaanxi Province of China (Grant No. 2025JC-YBQN-043).

## Conflict of Interest

The authors declare no conflict of interest.

## Data Availability Statement

The data that support the findings of this study are available from the corresponding author upon reasonable request.

## Keywords

hybrid integration, photonics integrated chip, quantum key distribution

Received: May 5, 2025
Revised: August 25, 2025
Published online:

[1] C. H. Bennett, G. Brassard, in *Proc. IEEE Int. Conf. Comp., Syst., Signal Process.* , India, IEEE, Piscataway, BJ **1984**, p. 175.
[2] F. Xu, X. Ma, Q. Zhang, H.-K. Lo, J.-W. Pan, *Rev. Mod. Phys.* **2020**, *92*, 025002.
[3] C. H. Bennett, F. Bessette, G. Brassard, L. Salvail, J. Smolin, *J. Cryptology* **1992**, *5*, 3.
[4] C. Z. Peng, J. Zhang, D. Yang, W. B. Gao, H. X. Ma, H. Yin, H. P. Zeng, T. Yang, X. B. Wang, J. W. Pan, *Phys. Rev. Lett.* **2007**, *98*, 010505.
[5] D. Rosenberg, J. W. Harrington, P. R. Rice, P. A. Hiskett, C. G. Peterson, R. J. Hughes, A. E. Lita, S. W. Nam, J. E. Nordholt, *Phys. Rev. Lett.* **2007**, *98*, 010503.
[6] T. Schmitt-Manderbach, H. Weier, M. Fürst, R. Ursin, F. Tiefenbacher, T. Scheidl, J. Perdigues, Z. Sodnik, C. Kurtsiefer, J. G. Rarity, A. Zeilinger, H. Weinfurter, *Phys. Rev. Lett.* **2007**, *98*, 010504.
[7] H. L. Yin, T. Y. Chen, Z. W. Yu, H. Liu, L. X. You, Y. H. Zhou, S. J. Chen, Y. Mao, M. Q. Huang, W. J. Zhang, H. Chen, M. J. Li, D. Nolan, F. Zhou, X. Jiang, Z. Wang, Q. Zhang, X. B. Wang, J. W. Pan, *Phys. Rev. Lett.* **2016**, *117*, 190501.
[8] A. Boaron, G. Boso, D. Rusca, C. Vulliez, C. Autebert, M. Caloz, M. Perrenoud, G. Gras, F. Bussières, M.-J. Li, D. Nolan, A. Martin, H. Zbinden, *Phys. Rev. Lett.* **2018**, *121*, 190502.
[9] S. K. Liao, W. Q. Cai, J. Handsteiner, B. Liu, J. Yin, L. Zhang, D. Rauch, M. Fink, J. G. Ren, W. Y. Liu, Y. Li, Q. Shen, Y. Cao, F. Z. Li, J. F. Wang, Y. M. Huang, L. Deng, T. Xi, L. Ma, T. Hu, L. Li, N. L. Liu, F. Koidl, P. Wang, Y. A. Chen, X. B. Wang, M. Steindorfer, G. Kirchner, C. Y. Lu, R. Shu, et al., *Phys. Rev. Lett.* **2018**, *120*, 030501.
[10] S. Wang, Z.-Q. Yin, D.-Y. He, W. Chen, R.-Q. Wang, P. Ye, Y. Zhou, G.-J. Fan-Yuan, F.-X. Wang, W. Chen, Y.-G. Zhu, P. V. Morozov, A. V. Divochiy, Z. Zhou, G.-C. Guo, Z.-F. Han, *Nat. Photonics* **2022**, *16*, 154.
[11] Y. Liu, W.-J. Zhang, C. Jiang, J.-P. Chen, D. Ma, C. Zhang, W.-X. Pan, H. Dong, J.-M. Xiong, C.-J. Zhang, H. Li, R.-C. Wang, C.-Y. Lu, J. Wu, T.-Y. Chen, L. You, X.-B. Wang, Q. Zhang, J.-W. Pan, *Quantum Front.* **2023**, *2*, 16.
[12] Y. Li, W.-Q. Cai, J.-G. Ren, C.-Z. Wang, M. Yang, L. Zhang, H.-Y. Wu, L. Chang, J.-C. Wu, B. Jin, H.-J. Xue, X.-J. Li, H. Liu, G.-W. Yu, X.-Y. Tao, T. Chen, C.-F. Liu, W.-B. Luo, J. Zhou, H.-L. Yong, Y.-H. Li, F.-Z. Li, C. Jiang, H.-Z. Chen, C. Wu, X.-H. Tong, S.-J. Xie, F. Zhou, W.-Y. Liu, Y. Ismail, et al., *Nature* **2025**, *640*, 47.
[13] M. Sasaki, M. Fujiwara, H. Ishizuka, W. Klaus, K. Wakui, M. Takeoka, S. Miki, T. Yamashita, Z. Wang, A. Tanaka, K. Yoshino, Y. Nambu, S. Takahashi, A. Tajima, A. Tomita, T. Domeki, T. Hasegawa, Y. Sakai, H. Kobayashi, S. M. Assad, K. Shimizu, T. Tokura, T. Tsurumaru, M. Matsui, T. Honjo, K. Tamaki, H. Takesue, Y. Tokura, J. F. Dynes, A. R. Dixon, et al., *Opt. Express* **2011**, *19*, 10387.


© 2025 Wiley-VCH GmbH

18638899, 0, Downloaded from https://onlinelibrary.wiley.com/doi/10.1002/lpor.202501080 by Shenghai Liao - University Of British Columbia , Wiley Online Library on [29/09/2025]. See the Terms and Conditions (https://onlinelibrary.wiley.com/terms-and-conditions) on Wiley Online Library for rules of use; OA articles are governed by the applicable Creative Commons License

[14] S. Nauerth, F. Moll, M. Rau, C. Fuchs, J. Horwath, S. Frick, H. Weinfurter, *Nat. Photonics* **2013**, *7*, 382.
[15] J. Y. Wang, B. Yang, S. K. Liao, L. Zhang, Q. Shen, X. F. Hu, J. C. Wu, S. J. Yang, H. Jiang, Y. L. Tang, B. Zhong, H. Liang, W. Y. Liu, Y. H. Hu, Y. M. Huang, B. Qi, J. G. Ren, G. S. Pan, J. Yin, J. J. Jia, Y. A. Chen, K. Chen, C. Z. Peng, J. W. Pan, *Nat. Photonics* **2013**, *7*, 387.
[16] Y. L. Tang, H. L. Yin, Q. Zhao, H. Liu, X. X. Sun, M. Q. Huang, W. J. Zhang, S. J. Chen, L. Zhang, L. X. You, Z. Wang, Y. Liu, C. Y. Lu, X. Jiang, X. Ma, Q. Zhang, T. Y. Chen, J. W. Pan, *Phys. Rev. X* **2016**, *6*, 011024.
[17] S. K. Liao, H. L. Yong, C. Liu, G. L. Shentu, D. D. Li, J. Lin, H. Dai, S. Q. Zhao, B. Li, J. Y. Guan, W. Chen, Y. H. Gong, Y. Li, Z. H. Lin, G. S. Pan, J. S. Pelc, M. M. Fejer, W. Z. Zhang, W. Y. Liu, J. Yin, J. G. Ren, X. B. Wang, Q. Zhang, C. Z. Peng, J. W. Pan, *Nat. Photonics* **2017**, *11*, 509.
[18] S. K. Liao, W. Q. Cai, W. Y. Liu, L. Zhang, Y. Li, J. G. Ren, J. Yin, Q. Shen, Y. Cao, Z. P. Li, F. Z. Li, X. W. Chen, L. H. Sun, J. J. Jia, J. C. Wu, X. J. Jiang, J. F. Wang, Y. M. Huang, Q. Wang, Y. L. Zhou, L. Deng, T. Xi, L. Ma, T. Hu, Q. Zhang, Y. A. Chen, N. L. Liu, X. B. Wang, Z. C. Zhu, C. Y. Lu, et al., *Nature* **2017**, *549*, 43.
[19] J. F. Dynes, A. Wonfor, W. W. Tam, A. W. Sharpe, R. Takahashi, M. Lucamarini, A. Plews, Z. L. Yuan, A. R. Dixon, J. Cho, Y. Tanizawa, J. P. Elbers, H. Greißer, I. H. White, R. V. Penty, A. J. Shields, *npj Quantum Inf.* **2019**, *5*, 101.
[20] Y. A. Chen, Q. Zhang, T. Y. Chen, W. Q. Cai, S. K. Liao, J. Zhang, K. Chen, J. Yin, J. G. Ren, Z. Chen, S. L. Han, Q. Yu, K. Liang, F. Zhou, X. Yuan, M. S. Zhao, T. Y. Wang, X. Jiang, L. Zhang, W. Y. Liu, Y. Li, Q. Shen, Y. Cao, C. Y. Lu, R. Shu, J. Y. Wang, L. Li, N. L. Liu, F. Xu, X. B. Wang, et al., *Nature* **2021**, *589*, 214.
[21] Y. Li, S.-K. Liao, Y. Cao, J.-G. Ren, W.-Y. Liu, J. Yin, Q. Shen, J. Qiang, L. Zhang, H.-L. Yong, J. Lin, F.-Z. Li, T. Xi, L. Li, R. Shu, Q. Zhang, Y.-A. Chen, C.-Y. Lu, N.-L. Liu, X.-B. Wang, J.-Y. Wang, C.-Z. Peng, J.-W. Pan, *Optica* **2022**, *9*, 933.
[22] C. Ma, W. D. Sacher, Z. Tang, J. C. Mikkelsen, Y. Yang, F. Xu, T. Thiessen, H.-K. Lo, J. K. S. Poon, *Optica* **2016**, *3*, 1274.
[23] P. Sibson, J. E. Kennard, S. Stanisic, C. Erven, J. L. O'Brien, M. G. Thompson, *Optica* **2017**, *4*, 172.
[24] P. Sibson, C. Erven, M. Godfrey, S. Miki, T. Yamashita, M. Fujiwara, M. Sasaki, H. Terai, M. G. Tanner, C. M. Natarajan, R. H. Hadfield, J. L. O'Brien, M. G. Thompson, *Nat. Commun.* **2017**, *8*, 13984.
[25] T. K. Paraïso, I. De Marco, T. Roger, D. G. Marangon, J. F. Dynes, M. Lucamarini, Z. Yuan, A. J. Shields, *npj Quantum Inf.* **2019**, *5*, 42.
[26] F. X. Wang, W. Wang, R. Niu, X. Wang, C. L. Zou, C. H. Dong, B. E. Little, S. T. Chu, H. Liu, P. Hao, S. Liu, S. Wang, Z. Q. Yin, D. Y. He, W. Zhang, W. Zhao, Z. F. Han, G. C. Guo, W. Chen, *Laser Photonics Rev.* **2020**, *14*, 1.
[27] H. Semenenko, P. Sibson, A. Hart, M. G. Thompson, J. G. Rarity, C. Erven, *Optica* **2020**, *7*, 238.
[28] K. Wei, W. Li, H. Tan, Y. Li, H. Min, W.-J. Zhang, H. Li, L. You, Z. Wang, X. Jiang, T.-Y. Chen, S.-K. Liao, C.-Z. Peng, F. Xu, J.-W. Pan, *Phys. Rev. X* **2020**, *10*, 031030.
[29] G. Zhang, J. Y. Haw, H. Cai, F. Xu, S. M. Assad, J. F. Fitzsimons, X. Zhou, Y. Zhang, S. Yu, J. Wu, W. Ser, L. C. Kwek, A. Q. Liu, *Nat. Photonics* **2019**, *13*, 839.
[30] L. Cao, W. Luo, Y. X. Wang, J. Zou, R. D. Yan, H. Cai, Y. Zhang, X. L. Hu, C. Jiang, W. J. Fan, X. Q. Zhou, B. Dong, X. S. Luo, G. Q. Lo, Y. X. Wang, Z. W. Xu, S. H. Sun, X. B. Wang, Y. L. Hao, Y. F. Jin, D. L. Kwong, L. C. Kwek, A. Q. Liu, *Phys. Rev. Appl.* **2020**, *14*, 011001.
[31] J. Dai, L. Zhang, X. Fu, X. Zheng, L. Yang, *Opt. Lett.* **2020**, *45*, 2014.
[32] Y. Ding, D. Bacco, K. Dalgaard, X. Cai, X. Zhou, K. Rottwitt, L. K. Oxenløwe, *npj Quantum Inf.* **2017**, *3*, 1.
[33] Y. Du, X. Zhu, X. Hua, Z. Zhao, X. Hu, Y. Qian, X. Xiao, K. Wei, *Chip* **2022**, *2*, 100039.
[34] L. Kong, Z. Li, C. Li, L. Cao, Z. Xing, J. Cao, Y. Wang, X. Cai, X. Zhou, *Opt. Express* **2020**, *28*, 18449.
[35] W. Pernice, F. Beutel, F. Brückerhoff-Plückelmann, H. Gehring, V. Kovalyuk, G. Goltsman, philipp Zolotov, *Optica* **2022**, *9*, 10.
[36] G. W. Zhang, W. Chen, G. J. Fan-Yuan, L. Zhang, F. X. Wang, S. Wang, Z. Q. Yin, D. Y. He, W. Liu, J. M. An, G. C. Guo, Z. F. Han, *Sci. China Inf. Sci.* **2022**, *65*, 1.
[37] K. Wei, X. Hu, Y. Du, X. Hua, Z. Zhao, Y. Chen, C. Huang, X. Xiao, *Photonics Res.* **2023**, *11*, 1364.
[38] G. Guarda, D. Ribezzo, T. Occhipinti, A. Zavatta, D. Bacco, *Phys. Rev. A* **2024**, *110*, 042605.
[39] Y. Bian, Y. Pan, X. Xu, L. Zhao, Y. Li, W. Huang, L. Zhang, S. Yu, Y. Zhang, B. Xu, *Appl. Phys. Lett.* **2024**, *124*, 17.
[40] D. Bunandar, A. Lentine, C. Lee, H. Cai, C. M. Long, N. Boynton, N. Martinez, C. Derose, C. Chen, M. Grein, D. Trotter, A. Starbuck, A. Pomerene, S. Hamilton, F. N. Wong, R. Camacho, P. Davids, J. Urayama, D. Englund, *Phys. Rev. X* **2018**, *8*, 021009.
[41] M. Avesani, L. Calderaro, M. Schiavon, A. Stanco, C. Agnesi, A. Santamato, M. Zahidy, A. Scriminich, G. Foletto, G. Contestabile, M. Chiesa, D. Rotta, M. Artiglia, A. Montanaro, M. Romagnoli, V. Sorianello, F. Vedovato, G. Vallone, P. Villoresi, *npj Quantum Inf.* **2021**, *7*, 93.
[42] W. Li, L. Zhang, H. Tan, Y. Lu, S. K. Liao, J. Huang, H. Li, Z. Wang, H. K. Mao, B. Yan, Q. Li, Y. Liu, Q. Zhang, C. Z. Peng, L. You, F. Xu, J. W. Pan, *Nat. Photonics* **2023**, *17*, 416.
[43] C.-X. Zhu, Z.-Y. Chen, Y. Li, X.-Z. Wang, C.-Z. Wang, Y.-L. Zhu, F.-T. Liang, W.-Q. Cai, G. Jin, S.-K. Liao, C.-Z. Peng, *Phys. Rev. Appl.* **2022**, *17*, 64034.
[44] R. Sax, A. Boaron, G. Boso, S. Atzeni, A. Crespi, F. GrÜnenfelder, D. Rusca, A. Al-Saadi, D. Bronzi, S. Kupijai, H. Rhee, R. Osellame, H. Zbinden, *Photonics Res.* **2023**, *11*, 1007.
[45] Y. Zhu, X. Wang, C. Zhu, Z. Chen, Z. Huang, Z. Jin, Y. Li, F. Liang, S. Liao, C. Peng, G. Jin, *AIP Adv.* **2022**, *12*, 125025.
[46] Z.-Y. Chen, C.-X. Zhu, Z.-S. Huang, Y. Li, X.-Z. Wang, F.-T. Liang, G. Jin, W.-Q. Cai, S.-K. Liao, C.-Z. Peng, *Rev. Sci. Instrum.* **2023**, *94*, 104703.
[47] X. B. Wang, *Phys. Rev. Lett.* **2005**, *94*, 230503.
[48] H. K. Lo, X. Ma, K. Chen, *Phys. Rev. Lett.* **2005**, *94*, 230504.
[49] D. Rusca, A. Boaron, F. Grünenfelder, A. Martin, H. Zbinden, *Appl. Phys. Lett.* **2018**, *112*, 17.
[50] F. Grünenfelder, A. Boaron, D. Rusca, A. Martin, H. Zbinden, *Appl. Phys. Lett.* **2020**, *117*, 14.
[51] T. K. Paraïso, T. Roger, D. G. Marangon, I. De Marco, M. Sanzaro, R. I. Woodward, J. F. Dynes, Z. Yuan, A. J. Shields, *Nat. Photonics* **2021**, *15*, 850.
[52] H. Heo, M. K. Woo, C. H. Park, H. S. Jang, H. Hwang, H. Lee, M. K. Seo, S. Kim, H. Kwon, H. Jung, S. W. Han, *APL Photonics* **2025**, *10*, 031301.
[53] F. Beutel, H. Gehring, M. A. Wolff, C. Schuck, W. Pernice, *npj Quantum Inf.* **2021**, *7*, 40.
[54] Z. Yan, T. Shi, Y. Fan, L. Zhou, Z. Yuan, *Adv. Dev. Instrum.* **2023**, *4*, 0029.
[55] A. A. E. Hajomer, C. Bruynsteen, I. Derkach, N. Jain, A. Bomhals, S. Bastiaens, U. L. Andersen, X. Yin, T. Gehring, *Optica* **2024**, *11*, 1197.
[56] A. Govdeli, J. N. Straguzzi, Z. Yong, Y. Lin, X. Luo, H. Chua, G.-Q. Lo, W. D. Sacher, J. K. S. Poon, *npj Nanophotonics* **2024**, *1*, 2.
[57] X. Ren, Y. Zhao, Z. Yan, Y. Shi, Z. Yuan, L. Lin, H.-B. Sun, Y. Huang, W. Zhang, *Laser Photon. Rev.* **2025**, *19*, e00826.
[58] J. A. Dolphin, T. K. Paraïso, H. Du, R. I. Woodward, D. G. Marangon, A. J. Shields, *npj Quantum Inf.* **2023**, *9*, 1.
[59] G. Zhang, Z. Zhao, J. Dai, S. Yang, X. Fu, L. Yang, *J. Lightwave Technol.* **2022**, *40*, 2052.
[60] Z. Lin, Y. Gao, L. Zhou, H. Yuan, Y. Zhu, Z. Lin, W. Zhang, Y. Huang, X.-L. Cai, Z. Yuan, *Optica Quantum* **2025**, *3*, 195.


© 2025 Wiley-VCH GmbH

18638899, 0, Downloaded from https://onlinelibrary.wiley.com/doi/10.1002/lpor.202501080 by Shenglai Liao - University Of British Columbia , Wiley Online Library on [29/09/2025]. See the Terms and Conditions (https://onlinelibrary.wiley.com/terms-and-conditions) on Wiley Online Library for rules of use; OA articles are governed by the applicable Creative Commons License